Nanoscale

Accepted Manuscript

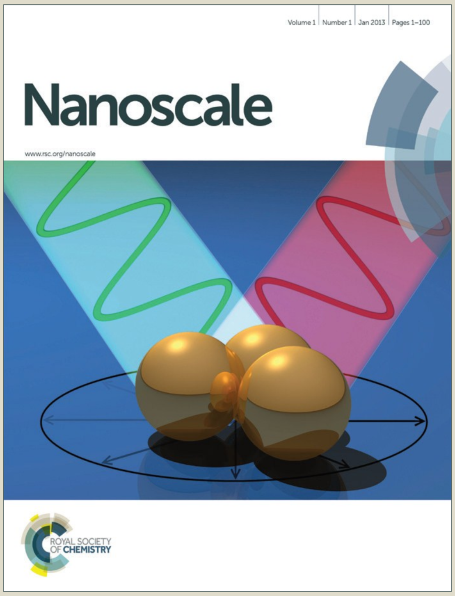

This is an *Accepted Manuscript*, which has been through the Royal Society of Chemistry peer review process and has been accepted for publication.

Accepted Manuscripts are published online shortly after acceptance, before technical editing, formatting and proof reading. Using this free service, authors can make their results available to the community, in citable form, before we publish the edited article. We will replace this *Accepted Manuscript* with the edited and formatted *Advance Article* as soon as it is available.

You can find more information about *Accepted Manuscripts* in the Information for Authors.

Please note that technical editing may introduce minor changes to the text and/or graphics, which may alter content. The journal's standard Terms & Conditions and the Ethical guidelines still apply. In no event shall the Royal Society of Chemistry be held responsible for any errors or omissions in this *Accepted Manuscript* or any consequences arising from the use of any information it contains.

ROYAL SOCIETY OF CHEMISTRY

www.rsc.org/nanoscale

Nanoscale

ARTICLE

Nanoscale Accepted Manuscript

Received 00th January 20xx,
Accepted 00th January 20xx

DOI: 10.1039/x0xx00000x

www.rsc.org/

Vanadium Nanobelts Coating Nickel Foam 3D Bifunctional Electrode with Excellent Catalytic Activity and Stability for Water Electrolysis

Yu Yu,[a] Pei Li,[a] Xiaofang Wang,[a] Wenyu Gao,[a] Zongxu Shen,[a] Yanan Zhu,[b] Shuliang Yang,[b] Weiguo Song,*[b] and Kejian Ding*[a]

Pursuit of highly active, stable and low-cost electrocatalysts for hydrogen evolution reaction (HER) and oxygen evolution reaction (OER) is the key point for large-scale water splitting. A vanadium nanobelts coating nickel foam (V/NF) is proposed as an excellent 3D bifunctional electrode for water electrolysis here, which exhibits high activities with overpotentials of 292 and 176 mV at 10 mA cm^{-2} for OER and HER respectively. When employed as bifunctional electrocatalysts in alkaline water electrolyzer, a cell voltage of 1.80 V was required to achieve 20 mA cm^{-2} with a slight increase during a 24-h durability testing. The existence of appropriate amount of nitrogen and oxygen elements in the surface region of vanadium nanobelts is regarded to be responsible for the electrocatalytic activity.

1. Introduction

As a highly expected substitute for the increasingly depleted fossil fuels, the clean, renewable, and abundant hydrogen resource has been urging constant endeavors from the industry and scientific research field.[1,2] Electrochemical water splitting has been regarded as the most effective technology to produce clean hydrogen fuel using the nearly no-cost water.[3,4] In spite of the theoretical water-splitting voltage of 1.23 V, this uphill reaction always requires quite large overpotential in the real applications.[5] Therefore, developing hydrogen evolution reaction (HER) and oxygen evolution reaction (OER) electrocatalysts with high efficiency, excellent durability and low expense is a top priority. Although the Pt, Ir, Ru precious metals and their clathrates/compounds were found as the highest active OER and HER catalysts,[6-8] their extensive usage was under severe restrictions due to their high cost and poor stability. Recently, tremendous exploration and development on highly efficient electrochemistry catalysts made from earth-abundant elements was achieved, both for HER (chalcogenides,[9-21] phosphides,[22-28] nitrides,[29,30] carbides,[31-33] et al[34-36]) and OER (oxides,[37-40] hybrid oxide,[41-45] hydroxides,[46-51] et al[52]).

When it comes to the practical electrochemical water splitting, HER and OER was reasonably requested to proceed in the same medium, to minimize the total overpotentials.[53] Strong acidic or alkaline electrolyte was always used to eliminate the potential loss caused by the pH gradient across the electrolyzer.[54] Most of the reported outstanding HER catalysts played well in acidic medium, but may inert or unstable toward alkalinity. In like manner, many preeminent OER catalysts at high pH may be inactive in acid, even suffer from the serious corrosion. A bifunctional catalyst synchronously with high efficiency towards both OER and HER was urgent to be developed. Comparatively, alkaline water splitting has a more favorable prospect, owing to its slighter destructive effect to catalysts and the more choices for catalysts.[5,55] In contrast to the masses of monofunctional catalysts, few bifunctional catalysts for both HER and OER (i.e. NiFe layered double hydroxide,[46] NiSe nanowire,[56] $NiCo_2S_4$ nanowire,[57] Ni_3N,[58] Co-P films[59]) were successfully fabricated. Herein, we present a vanadium nanobelts coating NF (V/NF) by a facial hydrothermal and subsequent annealing treatment, which played as an excellent 3D electrode in the electrolysis of water. The V/NF electrode exhibited fairly excellent electrocatalytic activity and stability in both of OER and HER under the alkaline condition. The overall water-splitting voltage at the current density of 20 mA cm^{-2} in the alkaline aqueous solution was required at 1.80 V, and this voltage displayed only a little rise of 30 mV during a 24-h durability test.

2. Experimental Section

2.1 Preparation of 3D vanadium nanobelts/nickel foam electrode (V/NF)

3D V/NF was prepared by a hydrothermal treatment and the sequent annealing at ammonia atmosphere. Firstly, a VO_2/NF

---

[a] *School of Sciences, Beijing Jiaotong University, No.3 Shangyuancun, Haidian District Beijing, 100044, P. R. China, E-mail: dkjian@bjtu.edu.cn*
[b] *Institute of Chemistry, Chinese Academy of Sciences, Zhongguancun North First Street 2, Beijing, 10009, P. R. China, E-mail: wsong@iccas.ac.cn*

Electronic Supplementary Information (ESI) available: More SEM, TEM imaes, XRD patterns, LSV curves, XPS spectra. See DOI: 10.1039/x0xx00000x framework was synthesized by a simultaneous hydrothermal synthesis and assembly procedure.[60] Detailedly, 25 mg V_2O_5 nanopowders were dispersed in 50 mL H_2O containing 1 mL H_2O_2 and formed an orange suspension by vigorous ultrasonication, and then transferred to a 100 mL Teflon-lined stainless steel autoclave. Six 1×4 cm^2 NF strips or a 24 cm^{-2} NF roll was perpendicularly placed in the suspension, to perform hydrothermal process at 180 °C for 1 h. After completion of the hydrothermal reaction, the as-prepared VO_2/NF was washed using deionized water and ethanol several times to remove residual ions and unsteadily attached VO_2. The dried VO_2/NF sample was experienced the calcination at 400 °C for 1 h under NH_3 flow, to convert VO_2/NF to V/NF. The heating rate was 10 °C min^{-1}.

2.2 Characterization

SEM images accompanied with EDS results and TEM images with the corresponding SAED (selected area electron diffraction) pattern were taken by scanning electron microscopy (SEM Hitachi-S4800) and transmission electron microscopy (TEM JEOL-2100F), respectively. Elements distribution mapping was also carried on SEM. XRay diffraction (XRD) patterns were recorded on a Rigaku diffractometer (Maxima XRD-7000) using Cu Ka irradiation. XPS information was obtained on a ESCALab220i-XL photoelectron spectroscopy. The mass loading density of V catalyst on NF was determinate by dissolving 3 cm^2 V/NF by 5 % hydrochloric acid, and measuring the solution by inductively coupled plasma optical emission spectrometer (Shimadzu ICP-9000).

2.3 Electrochemical measurements

All the electrochemical measurements were performed with a CHI760 electrochemical workstation (CH Instruments, Inc., Shanghai) in 1 M KOH alkaline solution. In the standard three-electrode system, a Pt net and SCE (saturated calomel electrode) were used as the counter electrode and reference electrode, respectively. The potential referred in this work was all at the reversible hydrogen electrode (RHE) scale, by the calibration according to following Equation: $E_{(RHE)} = E_{(SCE)} + 0.245\ V + 0.059 \times pH$. The linear sweep voltammetry (LSV) was carried at a scan rate of 2 mV s^{-1} to guarantee the reaction on the electrode to reach steady state. No activation was employed before the measurement, and the polarization curves with *iR*- compensation were adopted at 95 % level of ohmic potential drop. Electrochemical impedance spectroscopy measurements was conducted at - 0.20 and 1.65 V (vs RHE) for HER and OER respectively. To prepare the control sample of Pt-C/NF and IrO_2 with the same mass loading density as V/NF, quantitative Pt-C or IrO_2 was dispersed in 0.1 wt% Nafion ethanol solution to form an ink, and then uniformly dropped on NF followed by a vacuum drying. The electrolyte was previously saturated by the corresponding gas. The overall electrolysis of water was conducted in a two-electrode configuration, with a V/NF as both counter and reference electrodes and another identical V/NF as working electrode, and the voltage for EIS was adopted at 1.80 V.

3. Introduction

3.1 Fabrication of the V/NF 3D electrode

By the hydrothermal treatment of NF in the presence of V_2O_5 nanopodwers, the 3D NF was wrapped by a densely covering film consisting of masses of VO_2 nanobelts, with about 150 nm in width and more than several micrometers in length (Figure S4). In the optical photograph (Figure S1), it could be seen that NF with metallic luster transferred into a dark cyan appearance. This VO_2 nanobelts coating was reduced to vanadium after the annealing under NH_3 atmosphere, as the dark cyan precursor became black (Figure S1). The XRD patterns of final product (Figure 1a) demonstrated the existence of cubic vanadium phase (PDF#88-2322) with Fm3m space structure in this V/NF 3D electrode material. The diffraction peaks at 42.0 ° and 48.8 ° were indexed to the (111) and (200) facets of the metal vanadium phase, while strong peaks at 44.5, 51.8 and 76.4 ° corresponding to (111), (200), and (220) plane of metallic Ni phase was ascribed to its preponderant proportion. The peaks from other facets of vanadium were imperceptible owing to its weak crystallization and little content in the whole composite.

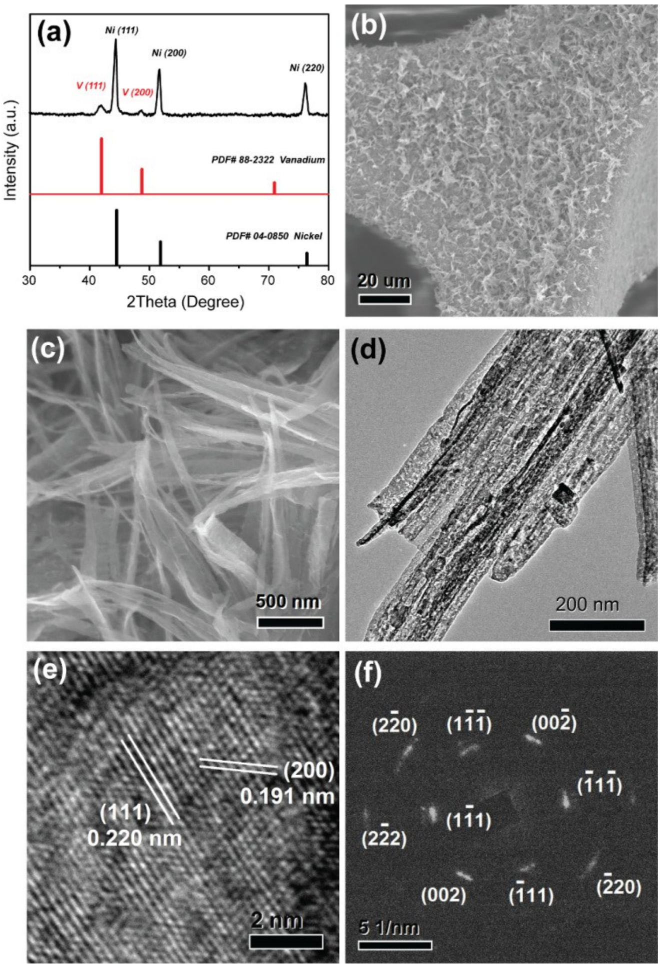

Figure 1. (a) XRD pattern, (b) low- and (c) high-resolution SEM images of V/NF electrode, (d) low- and (e) high-resolution TEM images, and (f) the corresponding SAED pattern of vanadium nanobetls.

Nanoscale Accepted Manuscript

This journal is © The Royal Society of Chemistry 20xx

Meanwhile, no signals originating from various vanadium oxides, nitride or oxynitride were detected from the expanded pattern (Figure S2b), indicating the mostly purity of the film on NF.

We also carried out an observation on the microcosmic morphology of V/NF by scanning electron microscopy (SEM). The large-scale and low-magnification SEM image (Figure S2a and 1b) showed that vanadium film was still fully and uniformity covering NF after annealing process. It was agreed with the mapping scanning for elements distribution as the vanadium elements bestrewed the whole framework of NF in Figure S3. Form the high magnification image (Figure 1c), vanadium was in maintenance of the nanobelts morphology, but displayed some extent of shrinkage due to the release of oxygen atoms. The widths of vanadium nanobelts distributed around 100 nm. Figure 1d presented the typical transmission electron microscopy (TEM) observation of the vanadium nanobelts aggregation, in which it could be seen that several belts formed a bundle-like structure owing to the phase transformation during the ammonia annealing, accompanied with the appearance of bumpiness and potholes on the surfaces of nanobelts. Even so, the high-resolution TEM image taken from an individual bumpy vanadium nanobelt and its corresponding selected area electron diffraction (SAED) pattern (Figure 1e and f) suggested its single crystal nature. The lattice fringes of vanadium (111) and (200) planes with interplanar distances of 0.220 and 0.190 nm respectively continually emerged in the whole belt, and the SAED pattern along with (110) zone axis displayed the spots indexed to {111} and {002} family of crystal planes. EDS study (Figure S2c) showed that V was one of the main elements in the composite, while strong Ni signal and some C were from NF and the carbon paste base respectively. It was worth noting that little N and O elements were also detected, which was in coincident with the results of elements mapping scanning. This implied that a small quantity of vanadium oxynitride was likely formed on the surface of vanadium nanobelts.[61,62]

Further, XPS analysis was employed to thoroughly survey the surface physicochemical property of vanadium nanobelts. As shown in V 2p spectrum (Figure 2a), by peak fitting, V elements were divided into four peaks corresponding to V^0 – V^{4+}.[63-66] Minor zero-valence V was detected while majority were partially oxidized to different extents, due to the existence of N and O interstitial dopants in the lattice of vanadium. It represented that some VN_xO_y component generated in the exterior region of the surface. Likewise, the broad V $2p_{1/2}$ peak at 519 - 526 eV could be also divided into dominated positively valent V and subordinate V^0 sub-peaks. The O 1s spectrum (Figure 2b) substantiated again the existence of O in the surface of vanadium nanobelts, in which the oxygen elements was classified into two types of structural O with low BE (binding energy) and adsorbed O with high BE. For the structural O, the BE of a small fraction at 529.9 eV was close to the common value in the vanadium oxide (about 530 eV), suggesting their bonding with V. Most of structural O atoms were covalently attached with N, giving a higher BE as 531.4 eV. [65,67,68] It was found oxygen species in the molecular, atomic or hydroxyl form had considerable affinity to the vanadium oxide and oxynitride,[63,68] and the oxygen adsorption also occurred in our work. The bonding of adsorbed O species to the surface was supposed to be favorable to related electrochemical reaction in the aqueous medium.[61,69]

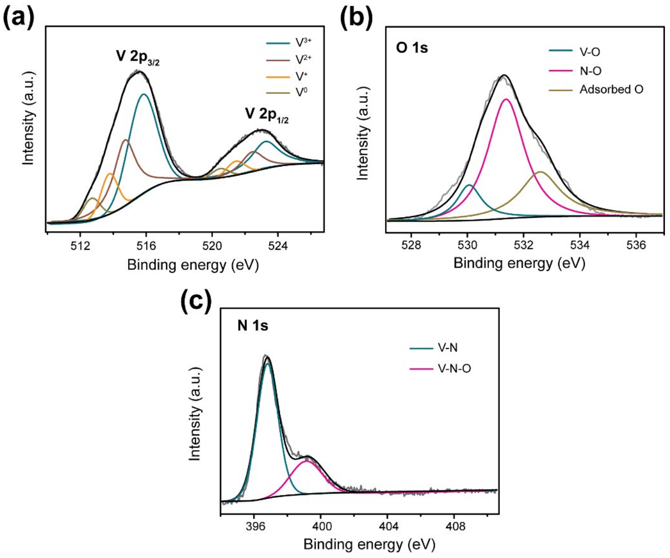

Figure 2. (a) V 2p, (b) O 1s, and (c) N 1s XPS spectra of vanadium nanobelts in V/NF electrode.

For N element, it was revealed in N 1s XPS spectrum (Figure 2c) that, there were also two different chemical binding types in VN_xO_y, detailedly, V-N and V-N-O (396.9 and 399.2 eV respectively).[62,70] Moreover, the higher-BE nitrogen ingredient was undetectable in the vanadium nanobelts, meaning that no other highly oxidized N was generated. The atomic percentages of V, N, and O elements derived from XPS were about 60, 24, and 16 % respectively. The proportions of N and O were both higher than the result by EDS (11 % for N and 4 % for O). Combining the the fact of the absence of individual vanadium oxide and nitride phases in V/NF by XRD characterization, it was reasonable to conclude that the N and O elements were mostly distributed in the crystal structure of metallic vanadium near the surface of vanadium nanobelts. The V/NF electrode was dissolved by HCl and measured by ICP-OES to determinate the mass loading density of vanadium nanobelts catalyst on NF, which was calculated as about 0.28 mg cm^{-2}.

3.2 Electrocatalytic performance for OER

To investigate the application in overall water-splitting of the V/NF 3D electrode, the OER electrocatalytic activity of V/NF was firstly measured in a three-electrode system with the saturated calomel electrode (SCE, in saturated NaCl) as reference electrode and Pt net as counter electrode. The linear sweep voltammetry (LSV) curves from negative to positive potential with *iR*-correction (95%, 0.25 Ω) in 1 M KOH at scan rate of 2 mV s^{-1} was shown in Figure 3a at the reversible hydrogen electrode (RHE) scale. For comparisons, OER polarization curves with *iR*-compensation of bare NF and IrO_2

Nanoscale Accepted Manuscript

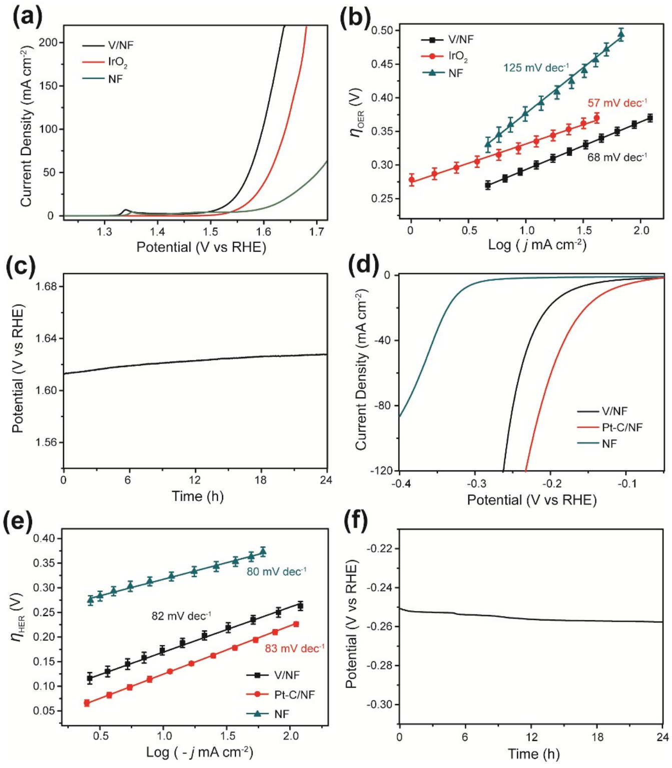

Figure 3. (a) OER polarization LSV curves and (b) Tafel plots of V/NF, IrO_2, and bare NF, (d) HER LSV curves and (e) Tafel plots of V/NF, Pt-C/NF, and NF. (c, f) Chronopotentiometric curve of V/NF at current density of 50 mA cm^{-2} for OER (c) and 20 mA cm^{-2} for HER without *iR*-correction. All experiments were carried out in 1.0 M KOH, and the LSV scan rates are 2 mV s^{-1}.

depositing NF with the same loading as V/NF were also measured. The V/NF electrode exhibited much superior performance to NF and IrO_2/NF. The onset potential of anodic reaction for V/NF was greatly more negative than that of NF, which was even slightly better than IrO_2/NF. An overpotential (η_{OER}) of 292 mV was required to achieve a current density of 10 mA cm^{-2}, 35 mV and 87 mV prior to IrO_2/NF and bare NF electrodes respectively. Compared to the previous reported OER electrocatalyst with high performance (Table S1),[37-41,43-47,49-51] V/NF showed competitive activity to some cases of the known best transitional metal layered double hydroxide[46-50] in the similar condition. Even before *iR*-correction, the overpotential for 10 mA cm^{-2} at 308 mV was also a quite low value (Figure S5). The superiority of V/NF was also observed in the corresponding Tafel plots (Figure 3b), in which V/NF gave a Tafel slope of 68 mV dec^{-1}, fantastically smaller than NF (127 mV dec^{-1}) and closed to IrO_2/NF (57 mV dec^{-1}), and the exchange current densities (j_0) of V/NF calculated by extrapolation of the Tafel plots to the J axis were 8.24 × 10^{-4} mA cm^{-2} significantly surpassed j_0 of IrO_2 (3.03 × 10^{-4} mA cm^{-2}). Electrochemical impedance spectroscopy (EIS) is another effective mean to analysize the kinetics of electrode process. As shown in Figure S7a, the charge transfer resistance (R_{ct}) from the semicircle in the low frequency zone of V/NF at 1.65 V (vs RHE) was only 1.23 Ω, smaller than that of IrO_2/NF (5.85 Ω), indicating a faster electron transfer and more facile electrocatalytic kinetics at the catalyst/electrolyte interface.

Not merely the activity, long-term running behavior was also an important consideration for the practical application. Chronopotentiometry measurement was employed to estimate the electrochemical stability of V/NF in OER. Figure 3c showed the chronopotentiometry curves of V/NF 3D electrode at the current density of 50 mA cm^{-2} in 1 M KOH. The applied potential was 1.613 V (without *iR*-correction) at the initial stage, and exhibited a slight increase to 1.628 V in a 24-h session. Besides, the V/NF electrode after 24-h stability testing was again LSV measured (Figure S8), and its original polarization curve presented only 7 mV positively shift compared to the fresh sample. Furthermore, the Tafel slope was even improved to 63 mV dec^{-1}, indicating the outstanding durability of V/NF in spite of the accumulation of oxygen in the electrolyte solution.

3.3 Electrocatalytic performance for HER

For the evaluating of the electrocatalytic HER performance of V/NF, the same three electrode system and electrolyte (1 M KOH) were adopted in the contrast of Pt-C/NF (20 wt%, with the same loading as V/NF) and bare NF, and LSV scan rate was also 2 mV s^{-1} to guarantee the reaction on the electrode to reach steady state. It was known that NF was of pretty electrocatalytic activity for HER, however like OER, V/NF behaved much more excellently than NF (Figure S6 and 3d). According to the LSV curves with *iR*-correction (95%, 0.67 Ω) in Figure 3d, the current density on V/NF achieved 10 and 20 mA cm^{-2} at the overpotentials (η_{HER}) of 176 and 203 mV respectively, while that on NF at these two overpotentials were only about 1.4 mA cm^{-2}. Although V/NF was revealed to be inferior in a subtle extent to Pt-C/NF, which required η_{HER} of only 125 mV for 10 mA cm^{-2}, its electrocatalytic activity for HER was better than or comparable to the many previous reported high-performance acid-applicable HER electrocatalysts (Table S2).[9-31,34-36] As shown in the Tafel plots (Figure 3e), the Tafel slope of V/NF (82 mV dec^{-1}) was quite analogous to that of Pt-C/NF (83 mV dec^{-1}). So the excellent HER kinetics was also obtained by the deposition vanadium nanobelts film on NF. j_0 of V/NF was calculated to 0.164 mA cm^{-2} for HER, although smaller than that of Pt-C/NF (0.5387 mA cm-2), it was also a comparatively large value and extremely bigger than NF. R_{ct} of V/NF at - 0.2 V (vs RHE) was estimated at 0.52 Ω (Figure S7a), showing some advantage against Pt-C/NF (0.74 Ω), suggesting its better kinetics.

As well the durability of V/NF was proved to be reliable by a 24-h chronopotentiometry testing at the current density of 20 mA cm^{-2} (Figure 3f), in which the required potential was slightly shifted from the initial 251 mV (without *iR*-correction) to 258 mV at the end. The outstanding durability of V/NF towards HER was confirmed by the LSV measurement of the sample after stability testing, as shown in Figure S9, a tiny negative shift of only 4 mV was observed, with a little increase of Tafel slope to 89 mV dec^{-1}.

3.4 Overall water-splitting

Nanoscale Accepted Manuscript

Please do not adjust margins

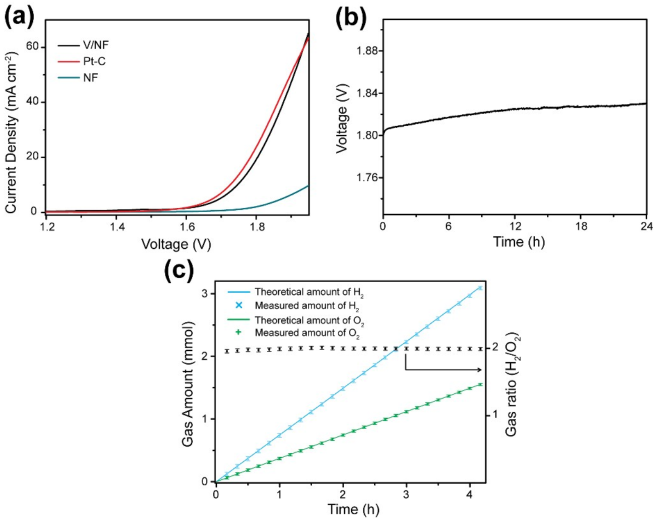

Figure 4 (a) LSV curves for water electrolysis of V/NF, Pt-C, and bare NF electrodes at scan rate of 2 mV s^{-1}. (b) Chronopotentiometric curve for water electrolysis of V/NF at density current of 20 mA cm^{-2}. All experiments were carried out in 1.0 M KOH, and the potentials was before the *iR*-correction.(c) The theoretical (lines) and measured (symbols) amounts of H_2 and O_2, and their ratios in the overall water-splitting.

As the above series of measurements revealed the high activity and stability of V/NF 3D electrode both for OER and HER in strongly basic media, electrolysis of water in a two-electrode configuration using V/NF as both anode and cathode was further carried to learn thoroughly about its real application. The V/NF based electrolyzer exhibited the close performance as the Pt-C/NF electrode, with the demand of a 1.74 V applying voltage to produce 10 mA cm^{-2} water-splitting current (Figure 4a). It was 210 mV lower and 14 mV higher than those of bare NF and Pt-C/NF respectively. However, V/NF exceeded Pt-C/NF in the larger current region, where the applying voltages for 60 mA cm^{-2} was asked as 1.91 V, 8 mV lower than Pt-C/NF. Meanwhile, R_{ct} of V/NF in the two-electrode system was investigated at the voltage of 1.80 (Figure S7b), which was quite small (1.38 Ω) compared to Pt-C/NF (11.4 Ω), indicating the prevail of V/NF on electrocatalytic kinetics over Pt-C/NF. Although the applied voltage for 10 mA cm^{-2} was higher than the electrocatalysts in other electrolyzers, i.e., NiFe layered double hydroxide (1.7 V),[46] NiSe nanowire (1.63 V),[56] $NiCo_2S_4$ nanowire (1.68 V),[57] Co-P films,[59] by taking loading mass into consideration (0.28 mg cm^{-2} in this work, almost 10 times more in other works, see Table S3), this V/NF 3D electrode could be regarded as competitive with others.

Like the individual HER and OER, V/NF exhibited robust durability for overall water splitting, as the applying voltage for 20 mA cm^{-2} underwent a little increase by only 27 mV (Figure 4b). The vigorous gas evolution on both electrodes was measured quantitatively by means of gas chromatography (GC). The generated O_2 and H_2 were maintaining at the ratio of ca. 2:1, and the amounts of them by both GC detection and theoretically calculation were shown in Figure 4c. The considerable coincidence of the experimental and theoretically values suggested the good bifunctional activities for OER and HER, with the Faradic efficiency (FE) of each at nearly 100%.

The stability of V/NF for HER and OER was found to be quite versatile. Specifically, the V/NF electrode not only maintained a high efficiency for HER and OER after respective stability test, but also was highly electrochemical active for the long-term counter reaction. The LSV polarization curve for OER from the V/NF electrode after 24-h HER was revealed to be a little preponderant to the initial sample, while its Tafel slope was improved to 63 mV dec^{-1} (Figure S8). The HER activity of V/NF after 24-h OER was in similar circumstances, as the majority of its LSV curve was prior to fresh sample, and the Tafel slope was 83 mV dec^{-1}, closed to fresh sample (Figure S9).

3.5 Analysis of surface characteristic

The material phase and surface characteristic of V/NF electrodes after the 24-h stability testing were investigated. The XRD patterns (Figure S10a and S11a) showed that, either after OER or HER, the component of the coating on the surface of NF was constant of vanadium phase, although both of their diffraction intensities were weakened to a certain extent. In addition, no other new phases including $Ni(OH)_2$ and NiO were found in spite of long-term OER or HER. For V/NF after 24-h OER, the V 2p XPS spectrum (Figure S10b) only showed the single $2p_{3/2}$ and $2p_{1/2}$ peaks at 516.4 and 524.0 eV respectively, attended by the vanishment of the original peaks. It meant that the surface vanadium elements were oxidized further to V^{4+} form V^0 - V^{3+},[63-66] which was caused by the diffusion of O species into the crystal lattice during the long-term electrochemical process in the aqueous media. Considering that the N elements was hard to be oxidized to gaseous nitrogen oxides (i.e. NO, NO_2, etc) or nitrogen molecules to be excluded out of the crystal structure, and the N 1s spectrum indeed declared the existence of N in the sample after 24-h OER, we speculated that with the O element, the oxidized N formed oxyacid anions NO_x^- containing N=O bond. As depicted in Figure S10d, besides N in V-N-O, the peaks at 403.4 and 407 eV was most likely assigned to nitrite and nitrate ions.[71,72] Simultaneously, the low-BE V-N peak disappeared. The O 1s spectrum (Figure S10c) showed that the peak of V-bonding structural O was greatly enhanced due to the increase of doped O, while a new peak for the double-bonding O in NO_x emerged.[65,67,68]. We could draw a conclusion that during the OER, except the oxidization of V^{3+} to V^{4+}, N element was also oxidized and partially formed polyoxy group. And the thickness of $VO(NO_x)$ component (not represent the real stoichiometric ratio) with higher crystal structural imperfection increased, compared to that of the initial VN_xO_y. In the HER stability testing, although a considerable negative potential was applied on V/NF, it was found that plenty of V was still oxidized to tetra-valence due to its long-term exposure aqueous medium (Figure S11b). Nevertheless, the metallic V could be detected. As shown in Figure S11c, the proportion of low-BE oxygen bonding with vanadium and constructing NO_x in the $VO(NO_x)$ was observably lower that that after OER. The N 1s spectrum (Figure S11d) pointed that, V-N bond was still existed,

Nanoscale Accepted Manuscript

Please do not adjust margins

Nanoscale Accepted Manuscript

V-N-O peak enhanced, and V-NO_x construction was also produced.

The impurity of the vanadium on the surface was regarded to be responsible for the outstanding catalytic activity for the electrochemical reactions in the aqueous media. Although the reaction mechanism is not clear, the different locations and bonging configuration of N and O in the crystal structure of V-N-O system, as well as the changeable valence of V, may bring V/NF the high activity for HER and OER. The possible promotion of electrocatalytic activity by Ni species of dopants was also excluded, as the the content of Ni element in the V nanobelt was about 0.13 %. We studied the water electrolysis performance of the VO_2/NF precursor, either for HER or OER, VO_2/NF exhibited poorer activity than V/NF (Figure S13). In the overall water-splitting, 1.84 V was required to reach 10 mA cm^{-2}, which was albeit higher than V/NF but substantially lower than bare NF. On the other hand, by prolonging the annealing time to 10 h, the metal vanadium on NF would be transformed into cubic vanadium nitride (VN) phase (Figure S12). VN/NF also presented a distinct inferior for OER to V/NF (Figure S13a). For HER, although VN/NF gave larger current densities in the lower overpotential region accompanied by capacitance effect, its kinetics was much worse than V/NF and VO_2/NF (Figure S13b). Capacitance effect was also observed in the overall water-splitting by VN/NF (Figure S13c), which brought VN/NF a closed applied voltage for 10 mA cm^{-2} compared to V/NF. By taking into consideration the difference in the surface areas of the three samples, we also take a comparation in the specific activity of V/NF, VO_2/NF and VN/NF versus their specific surface area. As shown in Fig. 13b, d, and e, the specific activity of V/NF revealed the superiority than those of VO_2/NF and VN/NF, in all of HER, OER and overall water splitting. It was worth noting that vanadium nitride was also inevitably partial oxidized on the surface, so it could be deduced that a tiny amount of oxygen elements also existed in the VN crystal structure with a smaller proportion (than in V/NF).

By the comparison of water electrolysis performances among V/NF, VO_2/NF, and VN/NF, we can concluded that oxygen elements in a tiny amount was adequate for the efficient electro-catalysis for HER, but a higher proportion was demanded for high activity for OER. The introduction of N elements was also of great importance, as the inexistence of N may significantly reduce the activities for both HER and OER, while the luxuriance of N went against the reaction kinetics in turn. Despite the existence of heteroatoms in the crystal lattice, the V nanobelts still kept metalline. For the metal and intermetal with d electrons, a high density of states at the Fermi level will bring about high catalytic activity.[73] It was theoretically and experimentally that, the 2p states of the nonmetal atom will participate in the hybridization of bands near the Fermi level, resulting in the increase of electron filling density and DOS.[74] So we speculated that there's a similar effect for the N and O interstitial atoms in the enhancement of the electrocatalytic activity of V nanobelts. In turn, if the V nanobelts were completely converted into nitride with the stoichiometric ratio, the activity dropped insteadly (Figure S13). It may correlate with the increase of the covalent fraction of the metal-nonmetal boding. The thorough mechanism will be explored in the following work.

Conclusions

In summary, a nanosized vanadium belts uniformly coating nickel foam 3D electrode was facilely synthesized by a hydrothermal and subsequent annealing treatment, which behaved as an excellent bifunctional electrode in the water electrolysis. The V/NF 3D electrode exhibited outstanding catalytic activity and durability for both OER and HER in strongly alkaline electrolyte, and achieved 20 mA cm^{-2} at a cell voltage of 1.80 V in overall water-splitting with a voltage rise of 30 mV after a 24-h continuous test. It was suggested reasonable amounts of nitrogen and oxygen elements were introduced on the surface of vanadium nanobelts, and the oxynitride layer was responsible for the electrocatalytic activity. This work not only demonstrated a highly promising candidate of electrode materials for scale-up application, but also opened up a new perspective extended the strategies for the noble-metal-free water electrolysis.

Acknowledgements

We gratefully thank the financial support by the National Natural Science Foundation of China (NSFC21503013, NSFC11079010), the Fundamental Research Funds for the Central Universities of China (2015JBM102, S13JB00200), the China Postdoctoral Science Foundation (2015M570922).

Notes and references

1. D. A. J. Rand and R. Dell, *Hydrogen energy: challenges and prospects*, Royal Society of Chemistry, 2008.
2. J. A. Turner, *Science*, 2004, **305**, 972-974.
3. T. E. Mallouk, *Nat. Chem.*, 2013, **5**, 362-363.
4. M. G. Walter, E. L. Warren, J. R. McKone, S. W. Boettcher, Q. Mi, E. A. Santori and N. S. Lewis, *Chem. Rev.*, 2010, **110**, 6446-6473.
5. K. Zeng and D. Zhang, *Prog. Energy Combust. Sci.*, 2010, **36**, 307-326.
6. W. Sheng, H. A. Gasteiger and Y. Shao-Horn, *J. Electrochem. Soc.*, 2010, **157**, B1529-B1536.
7. T. Reier, M. Oezaslan and P. Strasser, *ACS Catal.*, 2012, **2**, 1765-1772.
8. S. Trasatti, *J. Electroanal. Chem. Interfac.*, 1980, **111**, 125-131.
9. J. Yang, D. Voiry, S. J. Ahn, D. Kang, A. Y. Kim, M. Chhowalla and H. S. Shin, *Angew. Chem. Int. Ed.*, 2013, **52**, 13751-13754.
10. Y. Li, H. Wang, L. Xie, Y. Liang, G. Hong and H. Dai, *J. Am. Chem. Soc.*, 2011, **133**, 7296-7299.
11. Y.-F. Xu, M.-R. Gao, Y.-R. Zheng, J. Jiang and S.-H. Yu, *Angew. Chem. Int. Ed.*, 2013, **52**, 8546-8550.
12. D. Kong, H. Wang, Z. Lu and Y. Cui, *J. Am. Chem. Soc.*, 2014, **136**, 4897-4900.
13. C. G. Morales-Guio and X. Hu, *Acc. Chem. Res.*, 2014, **47**, 2671-2681.
14. X. Zhang, F. Meng, S. Mao, Q. Ding, M. J. Shearer, M. S. Faber, J. Chen, R. J. Hamers and S. Jin, *Energ. Environ. Sci.*, 2015, **8**, 862-868.
15. D. Kong, J. J. Cha, H. Wang, H. R. Lee and Y. Cui, *Energ. Environ. Sci.*, 2013, **6**, 3553-3558.

This journal is © The Royal Society of Chemistry 20xx

Please do not adjust margins

16. M.-R. Gao, Z.-Y. Lin, T.-T. Zhuang, J. Jiang, Y.-F. Xu, Y.-R. Zheng and S.-H. Yu, *J. Mater. Chem.*, 2012, **22**, 13662-13668.
17. M.-R. Gao, M. K. Y. Chan and Y. Sun, *Nat. Commun.*, 2015, **6**, 7493.
18. M.-R. Gao, J.-X. Liang, Y.-R. Zheng, Y.-F. Xu, J. Jiang, Q. Gao, J. Li and S.-H. Yu, *Nat. Commun.*, 2015, **6**, 5982.
19. Y.-R. Zheng, M.-R. Gao, Z.-Y. Yu, Q. Gao, H.-L. Gao and S.-H. Yu, *Chem. Sci.*, 2015, **6**, 4594-4598.
20. J. Duan, S. Chen, B. A. Chambers, G. G. Andersson and S. Z. Qiao, *Adv. Mater.*, 2015, **27**, 4234-4241.
21. S. Chen, J. Duan, Y. Tang, B. Jin and S. Zhang Qiao, *Nano Energy*, 2015, **11**, 11-18.
22. E. J. Popczun, C. G. Read, C. W. Roske, N. S. Lewis and R. E. Schaak, *Angew. Chem. Int. Ed.*, 2014, **53**, 5427-5430.
23. Q. Liu, J. Tian, W. Cui, P. Jiang, N. Cheng, A. M. Asiri and X. Sun, *Angew. Chem. Int. Ed.*, 2014, **53**, 6710-6714.
24. J. Tian, Q. Liu, A. M. Asiri and X. Sun, *J. Am. Chem. Soc.*, 2014, **136**, 7587-7590.
25. E. J. Popczun, J. R. McKone, C. G. Read, A. J. Biacchi, A. M. Wiltrout, N. S. Lewis and R. E. Schaak, *J. Am. Chem. Soc.*, 2013, **135**, 9267-9270.
26. P. Jiang, Q. Liu, Y. Liang, J. Tian, A. M. Asiri and X. Sun, *Angew. Chem. Int. Ed.*, 2014, **53**, 12855-12859.
27. X. Chen, D. Wang, Z. Wang, P. Zhou, Z. Wu and F. Jiang, *Chem. Commun.*, 2014, **50**, 11683-11685.
28. J. Kibsgaard and T. F. Jaramillo, *Angew. Chem. Int. Ed.*, 2014, **53**, 14433-14437.
29. B. Cao, G. M. Veith, J. C. Neuefeind, R. R. Adzic and P. G. Khalifah, *J. Am. Chem. Soc.*, 2013, **135**, 19186-19192.
30. W. F. Chen, K. Sasaki, C. Ma, A. I. Frenkel, N. Marinkovic, J. T. Muckerman, Y. Zhu and R. R. Adzic, *Angew. Chem. Int. Ed.*, 2012, **51**, 6131-6135.
31. W. Cui, N. Cheng, Q. Liu, C. Ge, A. M. Asiri and X. Sun, *ACS Catal.*, 2014, **4**, 2658-2661.
32. L. Liao, S. Wang, J. Xiao, X. Bian, Y. Zhang, M. D. Scanlon, X. Hu, Y. Tang, B. Liu and H. H. Girault, *Energ. Environ. Sci.*, 2014, **7**, 387-392.
33. Y. Zheng, Y. Jiao, Y. Zhu, L. H. Li, Y. Han, Y. Chen, A. Du, M. Jaroniec and S. Z. Qiao, *Nat. Commun.*, 2014, **5**, 3783.
34. H. Vrubel and X. Hu, *Angew. Chem.*, 2012, **124**, 12875-12878.
35. M. Gong, W. Zhou, M.-C. Tsai, J. Zhou, M. Guan, M.-C. Lin, B. Zhang, Y. Hu, D.-Y. Wang, J. Yang, S. J. Pennycook, B.-J. Hwang and H. Dai, *Nat. Commun.*, 2014, **5**, 4695.
36. J. Duan, S. Chen, M. Jaroniec and S. Z. Qiao, *ACS Catal.*, 2015, **5**, 5207-5234.
37. Y. Liang, Y. Li, H. Wang, J. Zhou, J. Wang, T. Regier and H. Dai, *Nat. Mater.*, 2011, **10**, 780-786.
38. X. Liu, W. Liu, M. Ko, M. Park, M. G. Kim, P. Oh, S. Chae, S. Park, A. Casimir, G. Wu and J. Cho, *Adv. Funct. Mater.*, 2015, **25**, 5799-5808.
39. T. Y. Ma, S. Dai, M. Jaroniec and S. Z. Qiao, *J. Am. Chem. Soc.*, 2014, **136**, 13925-13931.
40. M.-R. Gao, Y.-F. Xu, J. Jiang, Y.-R. Zheng and S.-H. Yu, *J. Am. Chem. Soc.*, 2012, **134**, 2930-2933.
41. T. Maiyalagan, K. A. Jarvis, S. Therese, P. J. Ferreira and A. Manthiram, *Nat. Commun.*, 2014, **5**, 3949.
42. F. Cheng, J. Shen, B. Peng, Y. Pan, Z. Tao and J. Chen, *Nat. Chem.*, 2011, **3**, 79-84.
43. Y. Zhu, W. Zhou, Z.-G. Chen, Y. Chen, C. Su, M. O. Tadé and Z. Shao, *Angew. Chem. Int. Ed.*, 2015, **54**, 3897-3901.
44. J.-I. Jung, H. Y. Jeong, J.-S. Lee, M. G. Kim and J. Cho, *Angew. Chem. Int. Ed.*, 2014, **53**, 4582-4586.
45. L. Kuai, J. Geng, C. Chen, E. Kan, Y. Liu, Q. Wang and B. Geng, *Angew. Chem. Int. Ed.*, 2014, **53**, 7547-7551.
46. J. Luo, J.-H. Im, M. T. Mayer, M. Schreier, M. K. Nazeeruddin, N.-G. Park, S. D. Tilley, H. J. Fan and M. Grätzel, *Science*, 2014, **345**, 1593-1596.
47. M. Gong, Y. Li, H. Wang, Y. Liang, J. Z. Wu, J. Zhou, J. Wang, T. Regier, F. Wei and H. Dai, *J. Am. Chem. Soc.*, 2013, **135**, 8452-8455.
48. L. Trotochaud, S. L. Young, J. K. Ranney and S. W. Boettcher, *J. Am. Chem. Soc.*, 2014, **136**, 6744-6753.
49. F. Song and X. Hu, *J. Am. Chem. Soc.*, 2014, **136**, 16481-16484.
50. X. Long, J. Li, S. Xiao, K. Yan, Z. Wang, H. Chen and S. Yang, *Angew. Chem. Int. Ed.*, 2014, **53**, 7584-7588.
51. S. Chen, J. Duan, P. Bian, Y. Tang, R. Zheng and S.-Z. Qiao, *Adv. Energy Mater.*, 2015, **5**, 1500936.
52. M. W. Kanan and D. G. Nocera, *Science*, 2008, **321**, 1072-1075.
53. E. A. Hernandez-Pagan, N. M. Vargas-Barbosa, T. Wang, Y. Zhao, E. S. Smotkin and T. E. Mallouk, *Energ. Environ. Sci.*, 2012, **5**, 7582-7589.
54. T. H. Sleutels, H. V. Hamelers, R. A. Rozendal and C. J. Buisman, *Int. J. Hydrogen Energy*, 2009, **34**, 3612-3620.
55. M. S. Burke, M. G. Kast, L. Trotochaud, A. M. Smith and S. W. Boettcher, *J. Am. Chem. Soc.*, 2015, **137**, 3638-3648.
56. C. Tang, N. Cheng, Z. Pu, W. Xing and X. Sun, *Angew. Chem.*, 2015, **127**, 9483-9487.
57. D. Liu, Q. Lu, Y. Luo, X. Sun and A. M. Asiri, *Nanoscale*, 2015, **7**, 15122-15126.
58. M. Shalom, D. Ressnig, X. Yang, G. Clavel, T. P. Fellinger and M. Antonietti, *J. Mater. Chem. A*, 2015, **3**, 8171-8177.
59. N. Jiang, B. You, M. Sheng and Y. Sun, *Angew. Chem. Int. Ed.*, 2015, **54**, 6251-6254.
60. S. Yang, Y. Gong, Z. Liu, L. Zhan, D. P. Hashim, L. Ma, R. Vajtai and P. M. Ajayan, *Nano Lett.*, 2013, **13**, 1596-1601.
61. D. Choi, G. E. Blomgren and P. N. Kumta, *Adv. Mater.*, 2006, **18**, 1178-1182.
62. X. Lu, M. Yu, T. Zhai, G. Wang, S. Xie, T. Liu, C. Liang, Y. Tong and Y. Li, *Nano Lett.*, 2013, **13**, 2628-2633.
63. G. Silversmit, D. Depla, H. Poelman, G. B. Marin and R. De Gryse, *J. Electron. Spectrosc. Relat. Phenom.*, 2004, **135**, 167-175.
64. N. Alov, D. Kutsko, I. Spirovova and Z. Bastl, *Surf. Sci.*, 2006, **600**, 1628-1631.
65. J. Kasperkiewicz, J. Kovacich and D. Lichtman, *J. Electron. Spectrosc. Relat. Phenom.*, 1983, **32**, 123-132.
66. A. Glaser, S. Surnev, F. Netzer, N. Fateh, G. Fontalvo and C. Mitterer, *Surf. Sci.*, 2007, **601**, 1153-1159.
67. E. Cazzanelli, G. Mariotto, S. Passerini, W. Smyrl and A. Gorenstein, *Sol. Energy Mater. Sol. Cells*, 1999, **56**, 249-258.
68. D. Shu, H. Cheng, C. Lv, M. A. Asi, L. Long, C. He, X. Zou and Z. Kang, *Int. J. Hydrogen Energy*, 2014, **39**, 16139-16150.
69. X. Zhou, H. Chen, D. Shu, C. He and J. Nan, *J. Phys. Chem. Solids*, 2009, **70**, 495-500.
70. R. Fix, R. G. Gordon and D. M. Hoffman, *Chem. Mater.*, 1993, **5**, 614-619.
71. J. F. Moulder, J. Chastain and R. C. King, *Handbook of X-ray photoelectron spectroscopy*, Perkin-Elmer Eden Prairie, MN, 1992.
72. D. Briggs, M. P. Seah and H. Bubert, *Practical Surface Analysis. Vol. 1*, Angewandte Chemie-German Edition, 1995.
73. S. T. Oyama, *Catal. Today*, 1992, **15**, 179-200.
74. L. I. Johansson, *Surf. Sci. Rep.*, 1995, **21**, 177-250.

Nanoscale Accepted Manuscript

Please do not adjust margins